

---

# Dosimetric Evaluation of Immunoscintigraphy Using Indium-111-Labeled Monoclonal Antibody Fragments in Patients with Ovarian Cancer

Wilhelmina C.A.M. Buijs, Leon F.A.G. Massuger, Roland A.M.J. Claessens, Peter Kenemans, and Frans H. M. Corstens

*Departments of Nuclear Medicine and Obstetrics and Gynecology, University Hospital Nijmegen, Nijmegen, The Netherlands*

---

This study reports the biodistribution and dosimetry for a monoclonal antibody against ovarian carcinoma. Eight patients received 140 MBq  $^{111}\text{In-OV-TL 3 F(ab')_2$ ; thereafter gamma camera imaging was performed daily up to 96 hr. By using the conjugated view counting method, activity in the organs was quantitated by phantom calibration and by whole-body measurements using a whole-body counter with the conjugated view counting method. Red bone marrow uptake was derived from regions of interest over the lumbar vertebrae and iliac crest. In both methods, organ uptake varied only slightly with time, having a mean value of approximately 18%, 4%, 6% and 17% of the injected dose in the liver, spleen, kidneys and red bone marrow, respectively. The mean radiation dose to these organs was 0.9, 1.5, 1.2 and 0.5 mGy/MBq. The effective dose equivalent was 0.4 mSv/MBq. In this study, two different methods of uptake calculations, result in similar values of organ uptake.

**J Nucl Med 1992; 33:1113-1120**

---

**R**adiolabeled monoclonal antibodies (Mabs) against tumor-associated antigens have been used to detect tumor deposits with variable degrees of success (1). Since gamma camera imaging of patients injected with radiolabeled Mabs has demonstrated selective tumor uptake of Mabs, antibody-directed radiotherapy has gained greater interest. Prior to employing antibodies for radioimmunotherapy, their biodistribution and dosimetry must be determined. The different characteristics of whole antibodies and fragments and of metallic and non-metallic radionuclides require that agents as similar as possible be used for dosimetry calculations and therapy. For instance, a biodistribution study with an iodinated whole antibody does not predict the radiation burden at therapy with  $^{90}\text{Y}$ -labeled  $\text{F(ab')}_2$  fragments.

We used an ovarian carcinoma-associated murine Mab, OV-TL 3, for the immunoscintigraphic detection of ovar-

ian cancer. The safety and diagnostic accuracy of imaging with the  $^{111}\text{In}$ -labeled OV-TL 3  $\text{F(ab')}_2$  was studied in 31 patients suspected for ovarian cancer (2). Several aspects of the biological behavior of the  $^{111}\text{In}$ -labeled Mab fragment in patients were studied using multiple blood samples and measurements of tissues removed at surgery (3). The latter study concentrated on tissue distribution of the radioimmunoconjugate at the time of surgery.

The aim of the current study was to determine the dynamic distribution of radioactivity over a number of organs and to calculate the radiation dose to these organs and to the total body. The technique most commonly used for quantitation of absolute organ activity is the conjugate view counting method with calculation of the geometric mean of the counts in opposing views of planar images (4, 5). Two different methods, both based on this principle, were evaluated. Both methods are modifications of existing techniques. In the first method, phantom-based correction factors were used to quantitate organ uptake (5,6). In the second method, calculated organ counts were compared with the amount of counts in the total body in order to obtain the absolute organ uptake (7). Data obtained for the liver using these methods were compared with measurements of activity in tissue specimens taken at surgery.

The radiation dose to various organs and the effective total body dose were estimated using the standard MIRD methods.

## MATERIALS AND METHODS

### Patients

Dosimetric studies were performed in 8 of 31 patients studied under a protocol approved by the Human Research Review Committee of this institution (2). Prior to study entry, each patient gave written informed consent. All eight patients were highly suspected of having primary or recurrent ovarian cancer and were scheduled to undergo subsequent surgery. The selection of these patients for inclusion in the study was based on the absence of large amounts of ascites in the abdomen and the fact that there was only minimal overlap of the liver, spleen and left kidney on the gamma camera images. The mean age of the patients was 62.1 yr (range: 50-77 yr). Indium-111-OV-TL 3  $\text{F(ab')}_2$  (1 mg, 140 MBq) in 5 ml of saline was intravenously

---

Received Jul. 15, 1991; revision accepted Jan. 10, 1992.  
For reprints contact: W.C.A.M. Buijs, MSc, Dept. Nuclear Medicine, University Hospital Nijmegen, 6500 HB Nijmegen, The Netherlands.

infused within 5 min. The actual administered dose was carefully measured prior to injection using a dose calibrator.

### Imaging Procedure

Planar gamma camera images were recorded 4, 24, 48, 72 and 96 hr after injection using a single-head gamma camera (Orbiter-ZLC-Digitrac, Siemens, Hoffmann Estates, IL) equipped with a parallel-hole medium-energy collimator and connected to a computer for subsequent data analysis (A<sup>2</sup>, Medical Data Systems/Medtronic, Ann Arbor, MI). Symmetric 20% windows were used for both the 173 and 247 keV energy peaks. At all time points, anterior and posterior planar images of the pelvis, abdomen and thorax were made with a 5-min preset time and stored in a 128 × 128 matrix. On average, a 5-min image recorded more than 500,000 events. Patients were imaged in the supine position with the gamma camera horizontally above or under the trunk.

### Urine and Feces Measurements

For 5 days following injection of the radiopharmaceutical, urine and feces were collected in 24-hr aliquots. Activity was measured in a well-type gamma counter and expressed as percent of the injected dose (%ID).

### Whole-Body Measurements

In one patient, the activity distribution in the body was measured with a shadow-shield whole-body counter in scan mode in order to assess the ratio of activity in the trunk to that in the total body.

### Quantitative Organ Uptake

Two methods were used to quantitate activity uptake in the liver, spleen and left kidney. In both methods, the conjugate view counting technique, using the geometric mean (GM) of counts in an organ, was used at various timepoints (4,5,8-11). The GM of anterior and posterior images was calculated according to the formula:

$$GM = \text{SORT} (A \times P),$$

where A is the number of counts in the anterior region and P is the number of counts in the posterior region. Prior to calculation of the GM, both anterior and posterior measurements were corrected for background. In Method 1, the absolute uptake of activity in an organ was calculated via comparison of the net (background-corrected) GM with a calibration curve obtained from measurements of known amounts of activity in a water equivalent phantom (5,6). In Method 2, the net GM in an organ was related to the GM of the total body using a combination of adjacent spot images to reconstruct a near whole-body GM (7).

### Background Correction

For each imaging study, regions of interest (ROIs) were manually drawn over the liver, spleen and left kidney on both anterior and posterior abdominal images. On the posterior image, the liver ROI excluded the overlying right kidney. Similar organ ROIs were chosen for all time points.

A background ROI was drawn over the area just caudally and medially of the left kidney. Background correction was performed on a counts per pixel basis. In order to avoid overcorrection, no background correction was performed for the liver, because this organ almost occupies the whole body thickness in cross section. For the spleen and kidney, only partial background correction was used (9). From x-ray CT scans, it was derived that these organs occupied only 30% of the whole-body thickness in cross

section, so a 70% value of the background ROI was subtracted to achieve this partial thickness compensation.

*Method 1 (Calibration Phantom).* In this method, the organ counts were calibrated with phantom measurements to correct for attenuation and scatter (5,6).

In calculating absolute organ activity, the GM of the anterior and posterior counts were corrected for gamma camera efficiency and for attenuation and scatter of gamma radiation in the patient (4). Gamma camera efficiency is defined as the count rate per unit activity without attenuation. The attenuation depends on patient thickness and tissue composition. Moreover, due to the scattered radiation, the degree of attenuation depends on the window settings of the gamma camera and the size of the ROI. The transmission curve, which describes the count rate from a source as a function of depth of the source in tissue, was measured for <sup>111</sup>In using two different source sizes. Cylindrical containers with a height of 3 cm and a diameter of 8.5 and 18 cm, respectively, were filled with water containing a known amount of <sup>111</sup>In. An attenuating phantom was built using acrylic plates with a diameter of 42 cm and a thickness of 2 or 3 cm. An additional partly hollow plate was constructed with a thickness of 4 cm, in which either one of the cylindrical sources at various depths could be placed, thus making it possible to image the cylindrical sources at various depths with steps of 1 cm up to a total depth of 21 cm.

Phantom measurements were performed with the same window settings used for patient imaging. For translation of acrylic thickness to tissue thickness, acrylic thickness was multiplied by 1.18, which represents the mass density of acrylic relative to tissue. The transmission factor, defined as the quotient of the count rate from a source with attenuation and the count rate from this source without attenuation, was calculated for various source depths. For a given patient thickness, the GM of the transmission factors for diverse combinations of source depths was calculated. The arithmetic mean of these GM values was used as correction factors for attenuation and scatter. These correction factors were computed for various patient thicknesses, ranging from 15 to 21 cm. The correction factors calculated for the large source were used to calibrate the GM counts of the liver. For the spleen, left kidney, lumbar spine and iliac crest, the transmission factors for the small source were used. The thickness of the abdomen was measured from x-ray CT scans. Because the thickness of the abdomen at the site of the right liver lobe and at the site of the spleen was smaller than the maximum thickness of the abdomen, a correction factor for a body thickness of 0.89 was used for the spleen and 0.91 for the liver (5). The absolute organ activity was calculated by dividing the GM of the organ counts by camera efficiency and the correction factor for attenuation and scatter. The percent uptake of the injected activity in that organ was calculated as the absolute organ uptake, corrected for physical decay and divided by the amount of injected activity.

*Method 2 (Whole Body).* This method calculates the percent organ uptake, relative to the total body activity, by using overlapping spot images to reconstruct near-whole body images (7,10,12). Total-body activity was measured by summing the GMs of adjacent body parts (thorax, abdomen and pelvis) after correction for differences in attenuation of these body parts. The difference in attenuation between the thorax, abdomen and pelvis was estimated with an <sup>111</sup>In transmission flood source in three patients. The count rate measured from the activity in the flood source after transmission through the patient was divided by the count rate of the flood source measured without attenuation by the patient. This quotient, the so called "transmission factor,"

was similar for both the abdomen and pelvis. The square root of the transmission factor for the thorax was on average 15% higher than that for both abdomen and pelvis transmissions. The thoracic contribution was multiplied by 0.85 in order to obtain correct total body counts. These calculated total-body counts were further corrected for that part of the body not seen by the gamma camera, as estimated from daily total-body profile scans with the shadow yield whole-body counter in one patient. The uptake of radioactivity in an organ at each time interval could then be calculated as the net GM divided by 1% of the corrected total-body counts and expressed as a percentage of the total-body counts at that time. Organ uptake as %ID was further corrected for the excretion of activity in urine and feces.

In all patients studied, subsequent surgery was performed between 5 and 7 days after infusion of the immunoconjugate. In three patients, liver biopsies of approximately 1 g of tissue were taken. All samples were weighed and  $^{111}\text{In}$  uptake was quantitatively measured using a well-type counter. Mean liver uptake was expressed as %ID/kg  $\pm$  s.d. and from these results total liver uptake was calculated, assuming a mean liver weight in elderly women of 1500 g. These results were compared with those obtained using ROI analysis.

### Red Bone Marrow

Uptake in the red bone marrow was estimated from the gamma camera images using calibration Method 1 with the small calibration source. Two different parts of the skeleton were chosen for measurement of red bone marrow uptake and the uptake found in each of these areas were extrapolated to the whole-body red bone marrow, assuming a homogenous distribution of the activity over the red bone marrow. A ROI was drawn around the lumbar vertebrae 13 + 14 together, corresponding with 4.6% of the total red bone marrow (13), and a background region of the same size was chosen adjacent to the left side of these vertebrae. Moreover, ROIs were drawn over a part of the left and right iliac crest. The sum of these areas represented 25% of the os coxae as calculated from x-ray CT measurements corresponding with 6.5% of total body red bone marrow (13). Background ROIs, the same size as those of the iliac crest, were drawn lateral to the iliac crest. For the lumbar vertebrae L3 + L4 and for the iliac crest, the GM was calculated from the background-corrected counts in the corresponding ROIs.

### Radiation Dose Calculation

Radiation absorbed dose to the organs was calculated with the MIRDOSE method (6,14). Revision 2 of a BASIC computer program (MIRDOSE2) was used with S-factors for 15-yr-old people (15). To obtain dose calculations in accordance with this method, the residence time in the source organs must be calculated. The liver, spleen, kidneys, red bone marrow, bladder and rest of the body were used as source organs. The amount of activity for the rest of the body at each time point was calculated as the difference between the injected activity and the sum of the excreted activity and the activity in the liver, spleen, both kidneys and red bone marrow. The residence time is defined as the cumulated activity in an organ per unit of injected activity and was calculated as the integration over time of the activity in an organ, not corrected for physical decay, divided by the amount of injected activity. It was assumed that uptake after 4 hr was representative as the initial uptake at time zero.

For the period from 0–96 hr, the trapezoidal method was used for the integration of activity over time. After 96 hr, it was

assumed that there was only physical decay and no increase or decrease of activity in the organs and the rest of the body. Residence times for the liver, spleen and the kidneys were calculated using the mean of the results obtained with Methods 1 and 2. For red bone marrow, the residence time was calculated as the mean of the results obtained for the vertebrae-derived red bone marrow uptake and the iliac crest-derived red bone marrow uptake. The residence time for the rest of the body was calculated as the mean of the results for each of the four combinations of Methods 1 and 2 and both red bone marrow uptake estimations. For the bladder, a constant urine flow and a voiding interval of 4 hr was assumed. The effective dose equivalent (EDE) was computed from the absorbed doses to the organs using weighting factors for adults, which represent the relative radiation sensitivity of organ or tissue (16).

## RESULTS

### Excretion in Urine and Feces

Urinary and fecal excretion of the radiolabel were measured in all eight patients studied. Total excretion (urine + feces) was at a relatively constant rate during the entire study period, where excretion of activity in the feces was small, compared to that in the urine. At 24, 48, 72 and 96 hr postinjection, the mean cumulative excretion was  $3.4 \pm 0.7$ ,  $8.1 \pm 1.5$ ,  $13.6 \pm 1.4$  and  $18.4 \pm 3.0$  %ID, respectively (Fig. 1).

### Whole-Body Measurements

During the study, there was a relative decrease in activity in those parts of the body not seen by the camera. When compared with the total body, the relative amount of counts in the trunk at 4, 24, 48, 72 and 96 hr was 85, 87, 88, 89 and 90%, respectively, meaning that there was a minimal shift in the distribution of the activity from the head and extremities to the trunk. The whole-body measurements in Method 2 were corrected accordingly.

### Organ Uptake

**Liver.** Liver uptake was calculated at five different time points during the study using both Methods 1 and 2 (Table

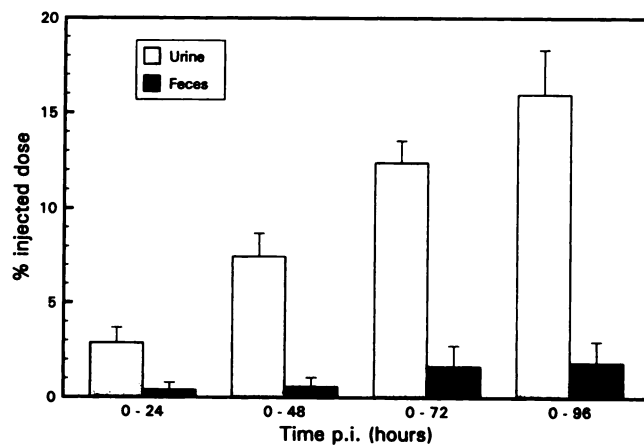


**FIGURE 1.** Cumulative excretion of urine and feces after injection of  $^{111}\text{In}$ -OV-TL 3 F(ab')<sub>2</sub>. Mean values (n = 8). Error bars represent 1 s.d.

**TABLE 1**  
Uptake of  $^{111}\text{In-OV-TL 3 F(ab')_2$  in the Liver According to Methods 1 and 2 (Results Are Expressed as %ID)

Patient no.	Time Postinjection				
	4 hr	24 hr	48 hr	72 hr	96 hr
Method 1					
1	19.0	18.6	19.3	18.7	19.9
2	15.6	17.2	17.9	16.6	16.6
3	12.5	13.6	13.4	12.6	13.7
4	25.9	30.8	29.3	28.4	26.8
5	16.3	17.4	17.2	14.9	15.9
6	16.5	17.7	19.3	15.7	15.7
7	12.1	14.4	14.2	13.2	14.1
8	12.2	11.9	11.5	10.9	10.0
mean	16.3	17.7	17.8	16.4	16.6
s.d.	4.3	5.4	5.1	5.1	4.7
Method 2					
1	19.2	18.0	19.2	18.2	19.0
2	18.9	19.9	20.4	19.1	18.9
3	14.6	15.6	15.7	14.7	15.5
4	25.8	31.1	30.1	28.7	27.8
5	17.3	17.9	17.1	16.1	15.1
6	17.3	19.9	19.9	18.5	17.7
7	15.2	17.8	17.4	16.9	16.9
8	15.1	15.0	14.3	13.2	12.8
mean	17.9	19.4	19.3	18.2	18.0
s.d.	3.4	4.7	4.5	4.4	4.2

**TABLE 2**  
Uptake of  $^{111}\text{In-OV-TL 3 F(ab')_2$  in the Spleen According to Methods 1 and 2 (Results Are Expressed as %ID)

Patient no.	Time postinjection				
	4 hr	24 hr	48 hr	72 hr	96 hr
Method 1					
1	4.9	4.6	4.2	3.8	3.6
2	7.7	7.3	5.5	5.8	4.7
3	6.4	4.8	3.9	3.7	4.2
4	4.2	3.4	3.1	2.6	2.7
5	3.9	3.4	3.5	3.0	3.1
6	3.6	3.0	3.7	3.0	3.2
7	7.9	6.3	5.9	5.3	5.0
8	5.5	3.3	2.9	2.7	3.0
mean	5.5	4.5	4.1	3.7	3.7
s.d.	1.6	1.5	1.0	1.1	0.8
Method 2					
1	4.1	3.7	3.4	3.1	2.9
2	7.7	7.1	5.3	5.8	4.5
3	6.4	4.7	3.8	3.7	4.0
4	3.5	2.8	2.6	2.2	2.3
5	3.3	2.7	2.8	2.6	2.3
6	3.2	2.9	3.2	3.0	3.1
7	8.4	6.6	6.1	5.7	5.0
8	5.9	3.6	3.1	2.8	3.2
mean	5.3	4.3	3.8	3.6	3.4
s.d.	1.9	1.6	1.2	1.3	0.9

1). Similar results were obtained with both methods. From 4 hr onwards, liver uptake was fairly constant during the entire 96-hr study period for all patients. Still, there were clear differences between patients for  $^{111}\text{In}$  uptake levels. At 24 hr, this level varied from 12% ID in Patient 8 to 31% ID in Patient 4. Mean liver uptake in all patients varied from  $16.3\% \pm 4.3\%$  to  $17.8\% \pm 5.1\%$  ID for Method 1 and from  $17.9\% \pm 3.4\%$  to  $19.4\% \pm 4.7\%$  ID for Method 2. Estimated liver uptake, using both ROI-based methods, was confirmed by tissue measurements taken in three patients at surgery. By assuming a mean liver weight of 1500 g, mean liver uptake ( $n = 3$ ) totaled  $19.1\% \pm 7.7\%$  ID. In these patients, mean liver uptake was  $20.1\% \pm 6.6\%$  ID, when calculated according to Method 1 and  $20.8\% \pm 6.3\%$  ID, when calculated according to Method 2.

**Spleen.** The calculated spleen uptake was also similar for both methods used (Table 2). Mean splenic uptake was highest at 4 hr postinfusion, being  $5.5\% \pm 1.6\%$  ID with Method 1 and  $5.3\% \pm 1.9\%$  ID with Method 2. Spleen uptake decreased during the study to  $3.7\% \pm 0.8\%$  ID (Method 1) and  $3.4\% \pm 0.9\%$  ID (Method 2) at 96 hr postinfusion. The level of spleen uptake at 24 hr postinjection varied between patients from approximately 3%–7% ID for both methods used.

**Kidneys.** Overall, calculated kidney uptake also demonstrated similar results for both methods used (Table 3). Kidney uptake for both kidneys was calculated as twice the measured uptake of the left kidney. Using both methods, there was a clear increase in kidney uptake from 4 hr

onwards. The highest mean uptake was measured at 48 hr, amounting to  $8.1\% \pm 2.4\%$  ID (Method 1) and  $6.7\% \pm 2.3\%$  ID (Method 2). After 48 hr, kidney levels decreased

**TABLE 3**  
Uptake of  $^{111}\text{In-OV-TL 3 F(ab')_2$  in the Kidneys According to Methods 1 and 2 (Results Are Expressed as %ID)

Patient no.	Time postinjection				
	4 hr	24 hr	48 hr	72 hr	96 hr
Method 1					
1	4.7	9.8	10.7	8.1	8.6
2	2.7	4.9	5.5	6.4	4.6
3	6.2	11.4	11.7	9.5	8.6
4	4.1	4.9	4.7	4.6	4.6
5	3.4	6.3	7.5	6.8	5.5
6	3.8	6.8	7.3	5.5	6.0
7	4.2	5.1	6.7	5.2	4.4
8	4.6	8.8	10.3	9.4	9.1
mean	4.2	7.4	8.1	6.9	6.4
s.d.	1.0	2.2	2.4	1.8	1.9
Method 2					
1	3.5	7.0	7.8	5.8	6.1
2	2.5	4.2	4.7	5.6	3.9
3	5.5	10.1	10.5	8.6	7.5
4	3.0	4.4	3.6	3.5	3.6
5	2.7	4.8	5.6	5.5	3.9
6	2.9	5.6	5.6	4.8	5.0
7	3.9	4.7	6.1	4.9	3.9
8	4.4	8.4	9.9	8.8	8.9
mean	3.6	6.2	6.7	5.9	5.4
s.d.	0.9	2.0	2.3	1.7	1.8

again, resulting in mean kidney levels of approximately 6% ID for both methods at 96 hr postinfusion.

**Red Bone Marrow.** Uptake in red bone marrow was calculated using Method 1 (Table 4). With both the iliac crest or two lumbar vertebrae as the ROI, similar results were obtained for total red bone marrow uptake. Mean red bone marrow uptake varied between  $13.9\% \pm 1.5\%$  and  $18.5\% \pm 4.6\%$  ID using the lumbar vertebrae, and between  $14.4\% \pm 2.1\%$  and  $18.9\% \pm 3.1\%$  ID using the iliac crest.

#### Radiation Dose Calculations

The residence times for the different source organs and the rest of the body are given in Table 5. The residence time for the bladder was assumed to be similar for all patients and was calculated to be 0.15 hr. The radiation dose to the different organs is given in Table 6. The mean calculated dose to the liver was  $0.86 \pm 0.19$ , spleen  $1.45 \pm 0.36$ , kidneys  $1.18 \pm 0.27$  and red bone marrow  $0.52 \pm 0.05$  mGy/MBq. For a typical administered amount of 140 MBq, this leads to a mean radiation dose of  $120 \pm 26$  mGy to the liver,  $202 \pm 51$  mGy to the spleen,  $165 \pm 38$  mGy to the kidneys and  $73 \pm 7$  mGy to the red bone marrow. The mean EDE was  $0.40 \pm 0.02$  mSv/MBq, or  $56.3 \pm 2.9$  mSv in the current study for an administered dose of 140 MBq  $^{111}\text{In-OV-TL 3 (Fab')}_2$ .

#### DISCUSSION

OV-TL 3, when radiolabeled with  $^{111}\text{In}$ , has already demonstrated its usefulness as an imaging agent in patients

**TABLE 4**  
Uptake of  $^{111}\text{In-OV-TL 3 F(ab')}_2$  in Total Red Bone Marrow Calculated via Lumbar Vertebrae and Iliac Crest (Results Are Expressed as %ID)

Patient no.	Time postinjection				
	4 hr	24 hr	48 hr	72 hr	96 hr
	Lumbar vertebrae				
1	15.0	15.5	15.2	14.8	16.9
2	14.5	14.6	12.5	14.4	17.8
3	15.6	26.8	22.1	23.3	21.4
4	14.6	9.2	8.8	10.8	9.1
5	11.0	19.9	20.1	23.6	22.3
6	14.7	24.5	22.4	22.2	15.0
7	13.8	14.9	15.2	16.7	15.2
8	11.7	17.9	23.5	22.3	18.1
mean	13.9	17.9	17.5	18.5	17.0
s.d.	1.5	5.3	5.0	4.6	3.9
	Iliac Crest				
1	10.4	16.3	13.8	17.4	23.2
2	14.8	14.7	12.3	16.0	13.7
3	17.4	15.1	14.0	13.9	19.4
4	13.4	16.6	16.6	21.4	17.7
5	14.2	17.6	17.3	14.4	15.5
6	15.5	13.5	16.3	15.6	17.8
7	13.0	15.3	19.2	14.0	21.2
8	16.6	15.7	20.5	25.7	22.4
mean	14.4	15.6	16.3	17.3	18.9
s.d.	2.1	1.2	2.6	3.9	3.1

**TABLE 5**  
Residence Times of  $^{111}\text{In-OV-TL 3 F(ab')}_2$  in Source Organs (Results Are Expressed in Hours)

Patient no.	Source organ				
	Liver	Spleen	Kidneys	Red bone marrow	Rest of body
1	18.7	3.6	7.3	16.8	39.8
2	17.7	5.6	4.4	14.5	43.9
3	14.1	4.3	8.7	19.1	39.9
4	27.8	2.7	4.2	13.3	38.1
5	16.0	2.9	5.0	17.8	44.4
6	17.3	3.1	5.4	17.2	43.2
7	15.1	5.7	4.6	16.3	44.4
8	12.1	3.3	8.4	19.2	43.0
mean	17.3	3.9	6.0	16.8	42.1
s.d.	4.4	1.1	1.7	1.9	2.3

suspected of having ovarian cancer (2). However, before pursuing therapeutic tumor targeting with this Mab labeled to  $^{90}\text{Y}$ , the therapeutic analog of  $^{111}\text{In}$ , a thorough assessment of the biodistribution in combination with dosimetry is indispensable.

Patients with ascites were omitted from the study, because of activity accumulation in ascites (3), making it impossible to determine the proper background activity. Furthermore, when ascites are present, lumbar vertebrae are hardly visible on anterior views. In the concept of the MIRD dose calculations, as used in this study, only a restricted number of source organs are selected. Abdominal volume with ascites cannot be defined as such. Activity in the ascites represents at most a smaller percent of the injected dose. Thus, it is very unlikely that concentration of activity in the source organs is significantly influenced by the presence or absence of ascites. Therefore, with respect to dose calculations, measurements in patients without ascites seem representative for the whole group of patients.

A variety of methods have been used to quantitate in vivo distribution of radioactivity (4-9,12,17-19). In most of these studies, the GM technique for conjugated views was used with one external calibration source for atten-

**TABLE 6**  
Radiation Doses for  $^{111}\text{In-OV-TL 3 F(ab')}_2$  in mGy/MBq

Patient no.	Organ					EDE (mSv/MBq)
	Liver	Spleen	Kidneys	Red bone marrow		
1	0.92	1.36	1.39	0.52	0.41	
2	0.87	2.00	0.93	0.47	0.41	
3	0.72	1.60	1.61	0.58	0.44	
4	1.30	1.04	0.90	0.44	0.38	
5	0.80	1.11	1.00	0.55	0.37	
6	0.85	1.18	1.07	0.53	0.38	
7	0.76	2.03	0.96	0.51	0.42	
8	0.64	1.27	1.55	0.59	0.41	
mean	0.86	1.45	1.18	0.52	0.40	
s.d.	0.19	0.36	0.27	0.05	0.02	

uation correction and estimation of gamma camera efficiency (5). An important drawback of this technique is its lack of correction for scatter (17,18). In order to overcome this problem, we used two different methods, both based on the GM technique for conjugate views.

In the first method (calibration phantom), mean organ counts were translated to activity (MBq) using two different calibration phantoms. In the second method (whole body), radioactivity in an organ was expressed as a percentage of whole-body radioactivity. In the latter method, the patient provides his own calibration, making correction for tissue attenuation, patient thickness and physical decay superfluous.

Despite efforts to optimize quantitation of absolute organ uptake, certain errors will be present. For Method 1, the phantoms should closely match the dimensions of the organs they represent (20,21). The phantoms we used were not ideal in that respect. Second, to compensate for scatter, we did not explicitly use a volume-dependent buildup factor (21). Since phantoms with different source sizes were measured at different depths and for diverse patient thicknesses, these determinations partially correct for scatter. The number of pixels in the ROI over the small source was similar to that in the ROIs over spleen, kidney, lumbar spine and iliac crest, 600–700 pixels in a  $128 \times 128$  matrix. The number of pixels in the ROI of the large source was about 2400, similar to the number of pixels found in the liver ROI. We therefore used the correction factors for attenuation and scatter of the small sources for the spleen, kidney, lumbar spine and iliac crest and the correction factors of the large source for the liver. For the small source, the correction factors for attenuation and scatter were 15%–20% lower in comparison to the large source. We thus concluded that a minor deviation in organ size, with respect to the source size used for calibration, may give an error in the estimation of absolute organ activity of no more than 5% of the calculated activity. Third, the homogeneous nonradioactive acrylic disks used as attenuation layers do not accurately reflect variations of tissue attenuation in the body. Fortunately, we were able to derive data on the thickness of the abdomen and on the individual sizes of organs from x-ray CT scans. However, in some investigations, these data will not be available.

For Method 2, several other sources of error may occur. First, accurate reconstruction of one close whole-body image from three adjacent spot images is difficult to perform and time-consuming. Second, the relative attenuation correction factor used for the thorax (0.85) was not assessed for each patient. The use of a special attenuation correction factor for the thorax seems adequate. However, the effect on the outcome will be relatively poor since counts in the thorax represent only one-quarter (at 4 hr postinjection) to one-seventh (at 96 hr postinjection) of the total body counts. Third, the relative contribution of counts from parts of the body not seen by the gamma

camera was measured in only one patient and used for the whole group. Another source of error may be the assumption that attenuation and scatter are similar for the total abdomen and the abdominal organs. This assumption may give an underestimation of organ uptake, because scatter contribution in the organ ROI is smaller than that for the total abdomen ROI. This effect is smaller for the liver in comparison with the other organs. Indeed, uptake in the kidneys seems to be lower, when calculated with Method 2 in comparison with Method 1.

The results were similar with both methods. From this study, no preference for either method can be made. However, it should be noted, that Method 2 is much more time-consuming.

The liver had the greatest uptake (approximately 19% ID). However, measurement of liver uptake can be erroneous for various reasons. Superimposition of the right kidney and/or the spleen results in a false elevation of the counts in the region. We excluded the right kidney from the liver ROI on the posterior image. Thus, a part of the liver does not contribute to the count rate on the posterior liver ROI, which underestimates the posterior count rate. The overestimation in the anterior liver counts might balance the under-estimation of the posterior counts when calculating the GM. Furthermore, the counts were not corrected for activity in the overlying red bone marrow in the ribs. In view of these variables, the direct measurements of tissue specimens of the liver (3) provided surprisingly similar results to those obtained with the gamma camera.

Uptake in the spleen was the lowest of all organs measured ( $\pm 4\%$  ID). Similar to the liver, spleen uptake was rather constant with time.

Because of great overlap of the right kidney with the liver on gamma camera images, only the absolute uptake in the left kidney was measured and calculated, assuming that the left kidney represented half of the activity in both kidneys at any time point. Increased activity in the kidneys was found up to 48 hr ( $\pm 8\%$  ID), whereas in both liver and spleen no increase of activity was measured during the study period.

The activity concentration was 0.01% ID/g for the liver and 0.02 and 0.025% ID/g for the spleen and the kidney. In vitro experiments using fluorescence-assisted cell sorter analysis have suggested a significant crossreactivity of OV-TL 3 with white blood cells (3). In vivo association of OV-TL 3 to blood cells, however, could never be detected in circulating blood. The relatively high and similar uptake of  $^{111}\text{In-OV-TL 3 F(ab')_2}$  in liver, spleen and kidneys points to uptake of liberated indium in these organs rather than significant crossreactivity of OV-TL 3 with leukocytes. The relatively high kidney uptake may in part be attributed to the excretion route of  $\text{F(ab')}_2$  fragments.

Two different ROIs (iliac crest and two lumbar vertebrae) were used to assess uptake in red bone marrow. Both regions resulted in similar estimations of the relative amount of uptake in the whole red bone marrow. Red

bone marrow uptake was rather high and increased slightly with time during the study. This finding has been previously described after injection of  $^{111}\text{In}$ -labeled  $\text{F(ab)}_2$  fragments of the Mab CA 19-9 by Hnatowich et al., who noted an increase in red bone marrow uptake on gamma camera images (22).

Both methods used to calculate marrow uptake have disadvantages. Extrapolation of the ROI data to the total amount of red bone marrow in the body can be done in different ways (13,23). Furthermore, lumbar vertebrae are often barely visible on anterior views and the superimposed aorta may interfere with the results. The orientation of the pelvis makes it rather difficult to draw the correct regions over the iliac crest for reproducible marrow mass measurements. For assessment of red bone marrow uptake, the sum of activity in bone and marrow within the ROI was used. The actual marrow uptake thus may be somewhat lower.

The purpose of this paper is to describe dose calculations for diagnostic imaging procedures and to derive an estimation of the absorbed dose in *normal* tissue. At surgery, several tissue specimens of tumor and liver were taken and activity was measured. These data were previously published (3). Total tumor uptake was 2%–5% of the injected activity at maximum. In this study, we did not include tumor dose calculations, due to a lack of exact knowledge of tumor mass, shape and location in the body. Moreover, in the MIRDOSE 2 program we used, only a restricted selection of source organs can be used as input.

In the literature, many studies report on the scintigraphic use of Mabs to detect ovarian cancer. However, few reports provide data on the quantitative uptake of the radiolabeled immunoconjugate in liver, spleen, kidneys etc. Harwood et al. used  $^{111}\text{In}$ -labeled B72.3 Mab, which reacts with different tumors, including ovarian tumors. In their study, uptake calculations for the liver were 32.1% ID, the spleen 3.9% ID, the kidneys 3.5% ID, and the lumbar spine marrow 2.7% ID (24). Uptake in the total red bone marrow can be calculated from extrapolation as 32% ID (13). Compared to our data, liver and red bone marrow uptake was higher, spleen uptake the same and kidney uptake was lower. However, they used an intact Mab, while we studied a  $\text{F(ab')}_2$  fragment. Beatty et al. (25,26) studied the uptake of  $^{111}\text{In}$ -labeled CEA Mab (Indacea) by measuring tissue samples. In two publications, within an interval of 4 yr, they reported a liver uptake of  $22.1\% \pm 3.2\%$  and  $20.3\% \pm 1.7\%$  ID/kg, respectively. For a mean liver weight of 1500 g, there was a total liver uptake of 33% and 30% ID, respectively, which is higher than the liver uptake found in our study. Hnatowich (22), who used the ROI method on scintigraphic images, found a mean liver uptake of  $20\% \pm 8\%$  ID at 24 hr after injection of  $^{111}\text{In}$ -labeled Mab (19-9)  $\text{F(ab')}_2$  fragment. This is similar to our results, giving a mean liver uptake of  $18\% \pm 5\%$  ID (Table 1).

For the calculation of activity residence time in the

organs, we assumed that the uptake at time 0 equals the measured uptake at 4 hr postinjection. Early images at 10–30 min after injection were made in a few patients. The calculated uptake was similar to the uptake measured at 4 hr postinjection in these patients. Therefore, the assumption seems to be valid. Moreover this assumption has only little effect on the calculated absorbed dose, due to the relatively long physical half-life of  $^{111}\text{In}$  and the slow biological disappearance of the activity from the organs.

For dose calculations, the most recent available version (January 1988) of the MIRDOSE dose computer program was used (27,28). In all patients, measurement of activity in blood samples at many time points was available. Regrettably, the program does not yet allow inclusion of the blood compartment as a separate source organ. The application of S-factors to 15-yr-old individuals and to adult women may result in a slight overestimation of the calculated absorbed doses in the organs and the total body. Also, the assumption that there is only physical decay for the time period after 96 hr postinjection may give an overestimation for the absorbed dose in the organs. This assumption seems reasonable, because for all organs, except the kidneys, uptake is constant over time. However, data for the kidneys suggest a biological disappearance of activity between 48 and 96 hr postinjection. If this decrease is representative for the period after 96 hr postinjection, the absorbed dose to the kidneys is overestimated by 10%–15%.

From the literature, very little data on absorbed dose to organs after administration of  $^{111}\text{In}$ -labeled Mabs are available. Taylor (29) and Macey (30) reported data on the Mab  $^{111}\text{In}$ -ZME-018. The absorbed dose in the liver, spleen, kidneys and bone marrow after administration of 2.5 mg Mab was 0.6, 1.5, 0.7 and 0.2 mGy/MBq, respectively (29). The whole-body dose was 0.13 mGy/MBq. We could derive a whole-body dose from our data, 0.17 mGy/MBq. Our data for liver and spleen are similar to their data, while their values for the kidneys and the bone marrow are lower. However, they have only limited data on bone marrow dosimetry (29). Fairweather (31) used  $^{111}\text{In}$ -CEA and found a whole-body dose of 0.135 mGy/MBq and a liver dose of 0.783 mGy/MBq. These numbers are similar to our results.

We calculated the effective dose equivalent (EDE) according to the method used in ICRP Publication 53 using the same weighting factors for adults (16), which makes it easy to compare the radiation burden of the Mab described in this study with that of other radiopharmaceuticals commonly used in nuclear medicine procedures. The EDE was 0.40 mSv/MBq, which was more than the 0.23 mSv/MBq for  $^{201}\text{Tl}$ -chloride and 0.12 mSv/MBq for  $^{67}\text{Ga}$ -citrate, two radiopharmaceuticals often used for tumor detection (16). For a typical 75 MBq dose of  $^{201}\text{Tl}$ -chloride, the EDE is 17 mSv; for a typical 185 MBq dose of  $^{67}\text{Ga}$ -citrate, the EDE is 22 mSv, whereas for a 140 MBq dose of  $^{111}\text{In}$ -OV-TL 3 ( $\text{Fab}'_2$ ), the EDE is 56 mSv.

With respect to the therapeutic use of Mabs, several problems need to be solved. The present chelators used to label Mabs with metallic radionuclides, such as  $^{111}\text{In}$  and  $^{90}\text{Y}$ , do not provide optimal stability of the radioimmunoconjugate (32,33), thus causing a relatively high uptake of activity in liver and bone (marrow) with a correspondingly high radiation burden. Furthermore, suboptimal chelate stability impairs the use of  $^{111}\text{In}$ -labeled antibodies in predicting the effect of therapy with  $^{90}\text{Y}$ -labeled Mabs.

## ACKNOWLEDGMENTS

The authors thank Mrs. Evelyn Watson for her critical review of the manuscript, H. Beekhuis for his advice in revising the manuscript and E. Koenders for technical assistance.

## REFERENCES

- Larson SM. Clinical radioimmuno detection, 1978-1988: overview and suggestions for standardization of clinical trials. *Cancer Res* 1990;50(suppl):892s-898s.
- Massuger LFAG, Kenemans P, Claessens RAMJ et al. Immunoscintigraphy of ovarian cancer with indium-111-labeled OV-TL 3 F(ab')<sub>2</sub> monoclonal antibody. *J Nucl Med* 1990;31:1802-1810.
- Massuger LFAG, Claessens RAMJ, Kenemans P, et al. Kinetics and biodistribution in relation to tumour detection with  $^{111}\text{In}$ -labelled OV-TL 3 F(ab')<sub>2</sub> in patients with ovarian cancer. *Nucl Med Commun* 1991;12:593-609.
- Thomas SR, Maxon HR, Kereiakes JG. In vivo quantitation of lesion radioactivity using external counting methods. *Med Phys* 1976;3:253-255.
- Fleming JS. A technique for the absolute measurement of activity using a gamma camera and computer. *Phys Med Biol* 1979;24:176-180.
- Beekhuis H, Nieweg OM. Radiation absorbed doses from Co-57-and Co-55-bleomycin. *J Nucl Med* 1984; 25:478-485.
- Reenen O van, Lötter MG, Heyns A, et al. Quantification of the distribution of  $^{111}\text{In}$ -labeled platelets in organs. *Eur J Nucl Med* 1982;7:80-84.
- Hammond ND, Moldofsky PJ, Beardsley MR, et al. External imaging techniques for quantitation of distribution of I-131 F(ab')<sub>2</sub> fragments of monoclonal antibody in humans. *Med Phys* 1984;11:778-783.
- Eary JF, Appelbaum FL, Durack L, et al. Preliminary validation of the opposing view method for quantitative gamma camera imaging. *Med Phys* 1989;16:382-387.
- Gainey MA, Siegel JA, Smergel M, et al. Indium-111-labeled white blood cells: dosimetry in children. *J Nucl Med* 1988;29:689-694.
- Moldofsky PJ, Powe J, Hammond ND. Monoclonal antibodies for radioimmunoimaging: current perspectives. *Nucl Med Ann* 1986:57-103.
- Rensburg AJ, Lötter MG, Heyns AP, et al. An evaluation of four methods of  $^{111}\text{In}$  planar image quantification. *Med Phys* 1988;15:853-861.
- ICRP Publication 23. *Report of the task group on reference man*. Oxford: Pergamon Press; 1975.
- Loevinger R, Berman M. A revised scheme for calculating the absorbed dose from biologically distributed radionuclides. *MIRD pamphlet no. 1, revised*. New York: Society of Nuclear Medicine; 1975.
- Vargo GJ. Software review: MIRDOSE, revision 2. *Health Phys* 1989;57:764.
- ICRP publication 53. *Radiation dose to patients from radiopharmaceuticals*. Oxford: Pergamon Press; 1988.
- Wu RK, Siegel JA. Absolute quantitation of radioactivity using the buildup factor. *Med Phys* 1984;11:189-192.
- Siegel JA, Wu RK, Maurer AH. The buildup factor: effect of scatter on absolute volume determination. *J Nucl Med* 1985;26:390-394.
- Myers MJ, Lavender JP, Oliveira JB, et al. A simplified method of quantitating organ uptake using a gamma camera. *Br J Radiol* 1981;54:1062-1067.
- DeVito RP, Hamill JJ, Treffert JD, et al. Energy-weighted acquisition of scintigraphic images using finite spatial filters. *J Nucl Med* 1989;30:2029-2035.
- Siegel JA. The effect of source size on the buildup factor calculation of absolute volume. *J Nucl Med* 1985;26:1319-1322.
- Hnатовich DJ, Griffin TW, Kosciuszky C, et al. Pharmacokinetics of indium-111-labeled monoclonal antibody in cancer patients. *J Nucl Med* 1985;26:849-858.
- Cristy M. Active bone marrow distribution as a function of age in humans. *Phys Med Biol* 1981;26:389-400.
- Harwood SJ, Carroll RG, Webster WB, et al. Human biodistribution of  $^{111}\text{In}$ -labeled B72.3 monoclonal antibody. *Cancer Res* 1990;50(suppl):932s-936s.
- Beatty JD, Duda RB, Williams LE, et al. Preoperative imaging of colorectal carcinoma with  $^{111}\text{In}$ -labeled anticarcinoembryonic antigen monoclonal antibody. *Cancer Res* 1986;46:6494-6502.
- Beatty JD, Williams LE, Yamauchi D, et al. Presurgical imaging with indium-labeled anti-carcinoembryonic antigen for colon cancer staging. *Cancer Res* 1990;59(suppl):922s-926s.
- Cloutier RJ, Watson EE, Rohrer RH, et al. Calculating the radiation dose to an organ. *J Nucl Med* 1973;14:53-55.
- Coffey JL, Watson EE. Calculating dose from remaining body activity: a comparison of two methods. *Med Phys* 1979;6:307-308.
- Taylor A, Milton W, Eyre H, et al. Radioimmuno-detection of human melanoma with indium-111-labeled monoclonal antibody. *J Nucl Med* 1988;29:329-337.
- Macey DJ, Denardo SJ, Denardo GL, Goodnight JK, Unger MW. Uptake of indium-111-labeled monoclonal antibody ZME-018 as a function of tumor size in a patient with melanoma. *Am J Physiologic Imaging* 1988;3:1-6.
- Fairweather DS, Bradwell AR, Dykes PW, Vaughan AT, Watson-James SF, Chandler S. Improved tumour localisation using indium-111 labelled antibodies. *Br Med J* 1983;287:167-170.
- Goldenberg DM. Future role of radiolabeled monoclonal antibodies in oncological diagnoses and therapy. *Semin Nucl Med* 1989;19:332-339.
- Roselli M, Schlom J, Gansow OA, et al. Comparative biodistributions of yttrium- and indium-labeled monoclonal antibody B72.3 in athymic mice bearing human colon carcinoma xenografts. *J Nucl Med* 1989;30:672-682.